Numerical Research on Effects Upon Precipitation Forecast of Doppler-Radar Estimated Precipitation and Retrieved Wind Field Under Different Model Initial Schemes*

WANG Yehong[1†](王叶红), ZHAO Yuchun[2] (赵玉春), and CUI Chunguang[1](崔春光)

1 *Wuhan Institute of Heavy Rain, CMA, Wuhan* 430074

2 *Wuhan Central Meteorological Observatory, Wuhan* 430074

(Received January 16, 2007)

ABSTRACT

On the basis of the joint estimated 1-h precipitation from Changde, Jingzhou, and Yichang Doppler radars as well as Wuhan digital radar, and the retrieved wind fields from Yichang and Jingzhou Doppler radars, a series of numerical experiments with an advanced regional η-coordinate model (AREM) under different model initial schemes, i.e., Grapes-3DVAR, Barnes objective analysis, and Barnes-3DVAR, are carried out for a torrential rain process occurring along the Yangtze River in the 24-h period from 2000 BT 22 July 2002 to investigate the effects of the Doppler-radar estimated rainfall and retrieved winds on the rainfall forecast. The main results are as follows: (1) The simulations are obviously different under three initial schemes with the same data source (the radiosounding and T213L31 analysis). On the whole, Barnes-3DVAR, which combines the advantages of the Barnes objective analysis and the Grapes-3DVAR method, gives the best simulations: well-simulated rain band and clear mesoscale structures, as well as their location and intensity close to observations. (2) Both Barnes-3DVAR and Grapes-3DVAR schemes are able to assimilate the Doppler-radar estimated rainfall and retrieved winds, but differences in simulation results are very large, with Barnes-3DVAR's simulation much better than Grapes-3DVAR's. (3) Under Grapes-3DVAR scheme, the simulation of 24-h rainfall is improved obviously when assimilating the Doppler-radar estimated precipitation into the model in compared with the control experiment; but it becomes a little worse when assimilating the Doppler-radar retrieved winds into the model, and it becomes worse obviously when assimilating the Doppler-radar estimated precipitation as well as retrieved winds into the model. However, the simulation is different under Barnes-3DVAR scheme. The simulation is improved to a certain degree no matter assimilating the estimated precipitation or retrieved winds, or both of them. The result is the best when assimilating both of them into the model. And (4) Barnes-3DVAR is a new and efficient initial scheme for assimilating the radar estimated rainfall and retrieved winds.

Key words: Doppler-radar, estimated precipitation, retrieved winds, assimilation, rainfall forecast

1. Introduction

Heavy rain, which is usually triggered by a series of severe meso-β or -γ convective systems (Tao, 1980), is one of main meteorological disasters. One way of forecasting heavy rain is mesoscale numerical model. Whether initial model field contains correct mesoscale information or not is a key factor in forecasting heavy rain. So far, the initial fields of mesoscale model are mainly from radiosoundings and background fields forecasted by large-scale weather model. Due to spatial sparseness, it is hard to catch mesoscale details of heavy rain systems, and therefore it is very difficult to forecast heavy rain accurately. In the last few years, with the enhancement of detection tools and improvement of detection technology, more and more data are available. For example, Doppler radar network in China has become an important observing network. Besides providing quantitative rainfall monitoring and disastrous weather nowcasting, Doppler radar detections, containing sufficient mesoscale information such as cloud, precipitation, and winds with high temporal and spatial resolution, are becoming an important data source for mesoscale model. How to apply these data into mesoscale numerical model effectively and sufficiently is a question needing to be solved as soon

*Supported by the Natural Science Foundation of Hubei under Grant No. 2003ABA009, the National "Ten-Five" Key Science and Technology Project under Grant No. 2001BA607B, and the "National Key Developing Program for Basic Science" Project under Grant No. 2004CB418307.

†Corresponding author: yehongw@whihr.com.cn.

as possible.

Since Gal-Chen (1978) firstly generated initial pressure field from winds with thermodynamic inversion technology and applied Doppler radar data into anelastic model, much progress in the assimilation of Doppler radar detections has been made in a short time. The meteorologists (Sun et al., 1991; Qiu and Xu, 1992; Shapiro et al., 1995; Tao, 1992) developed a series of technologies to retrieve wind vectors and temperature fields from Doppler radar detections. These technologies have laid a foundation for using Doppler radar data in numerical model. Shapiro et al. (1996) made forecasting experiments using initial fields generated from Doppler radar data based on wind vector inversion.

Sun et al. (1991, 1994, 1997, 1998) advanced a 4DVAR system to assimilate and retrieve Doppler radar data with four-dimensional variational method, cloud model, and its adjusting model, then improved the 4D-VDRAS (four-dimensional variational Doppler radar analysis system), checked it by gust wind data, and obtained a good result. Weygandt (1998) and Gao et al. (1998) initialized mesoscale numerical model with retrieved data from single Doppler radar and also got a hopeful result. Qiu et al. (2000) put up with a quasi-four-dimensional variational method to retrieve wind vectors from single-Doppler radar data, generated initial pressure field from winds with thermodynamic inversion technology presented by Gal-Chen (1978), and then made numerical experiments to forecast a squall-line storm system passing through Oklahoma with the Advanced Regional Prediction System (ARPS) developed by the Center for Analysis and Prediction of Storms (CAPS). The results indicate that the forecasts are improved obviously when Doppler radar data are assimilated into model initial fields. Ma et al. (2001) carried out single Doppler radar wind inversion and assimilation numerical experiments, which show that the application of retrieved horizontal winds into mesoscale numerical model helps to analyze and forecast meso- and micro-scale weather systems. Wang et al. (2004a, b) made one-dimensional variational assimilation of Doppler radar estimated rainfall by adjustment of humidity profiles, which indicates that using Doppler radar estimated rainfall into numerical model can improve heavy rainfall forecasting obviously. Wan et al. (2005) advanced a method for directly assimilating Doppler radar radial velocities and echo intensities in a variational assimilation frame and carried out numerical case studies.

In the last few years, the assimilation of Doppler radar data has been given more and more attention in the formation of model initial values. But as far as it goes, the Doppler radar data are not used efficiently in numerical weather forecast. Therefore, it is necessary to do further research.

During the period of 22-25 July 2002, a weather pattern of "two troughs and one ridge" is persistent and stable in the middle-high latitudes of East Asia with a cold trough dominating this area in the upper air and surface cold air surging to the south, a long-lasting heavy rain with high intensity occurred widely along the Yangtze River (see Shi et al., 2003). S-wave Doppler radar at Yichang and Changde and C-wave portable Doppler radar at Jingzhou detected the rainfall system with every-6-min volume scanning and obtained a large amount of detecting data. Xiao et al. (2005) retrieved hourly rainfall with detections of the three Doppler radars and Wuhan WSR-81S digital radar and then made a reflectivity mosaic. At the same time, Cheng et al. (2004) made a three-dimensional wind inversion with VVP (velocity volume processing) method and found that the heavy rain is generated by several meso-β systems embedded on a meso-α shear line in a favorable large-scale atmospheric circulation. In this paper, a three-dimensional variational assimilation is carried out to simulate the heavy rain in 24 h starting at 2000 BT (Beijing Time) 22 July 2002 with these radar-retrieved rainfall and winds, and to investigate the different effects of radar-estimated rainfall and radar-retrieved winds on rainfall forecast under three different model initial schemes.

2. Features of heavy rain on 22 July 2002

At 2000 BT 22 July 2002, a "two troughs and one ridge" weather pattern dominates stably in mid- and high-latitudes of Eurasia—two lows are in the east of

Ural Mountains and North China, respectively, with a high ridge in Baikal region as a blocking system. The West Pacific subtropical high is oriented southwestward-northeastward and stable, with its main body further east and north than normal. The mid-lower valleys of the Yangtze River are dominated by a wide trough and continuously influenced by eastward moving short waves from Baikal ridge (Fig.1, Zhao et al., 2003). Heavy rain is generated by the interaction between different scale weather systems under such a favorable large-scale circulation.

During the 24-h periods ending at 2000 BT 23 July, heavy rain occurred widely in the connecting areas of Hunan-Guizhou, Hunan-Hubei, Hubei-Henan-Anhui, and Jiangsu-Anhui, with 24-h rainfall more than 100 mm in over 20 observing stations (Fig.2). The 24-h rainfall at Dawu is 192.4 mm, with a maximum rain rate of 23.2 mm h^{-1}. The rain band is in an SW-NE orientation and mainly in Sinan, Yuanling, Jingzhou, Dawu, Yingshang, Bengbu, and Huaiyin, with several heavy rain centers in the vicinity of Sinan, Yuanling, Lixian, Jingzhou, Guangshui, Dawu, Yingshang, Bengbu, Huaiyin, and Sheyang. The maximum rainfall is in the middle of the rain band, with six rainstorm centers, i.e., Dawu, Yingshang, Guangshui, Bengbu, Yuanling, and Jingzhou, respectively. The rain mass is small and of typical meso-β-scale

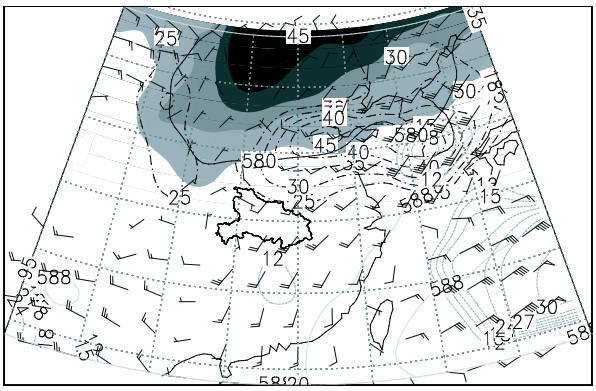

Fig.1. Synoptic scale systems and overlaid physical variables at 2000 BT 22 July 2002. The shading denotes $T \leqslant$-6°C area at 500 hPa, the dashed line for $|V| \geqslant$25 m s^{-1} at 200 hPa, the dotted line for $|V| \geqslant$ 12 m s^{-1} at 850-hPa, the solid 588-dagpm line for the characteristic line of the subtropical high, the 580-dagpm line for the position of 500-hPa troughs, and the barbed arrow for the wind at 700 hPa.

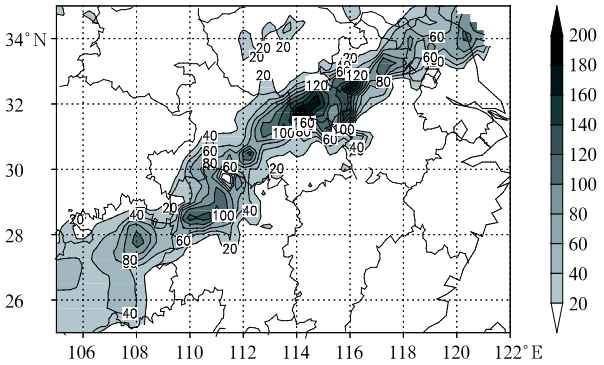

Fig.2. 24-h rainfall observed at 2000 BT 23 July 2002 (the contour interval is 20 mm).

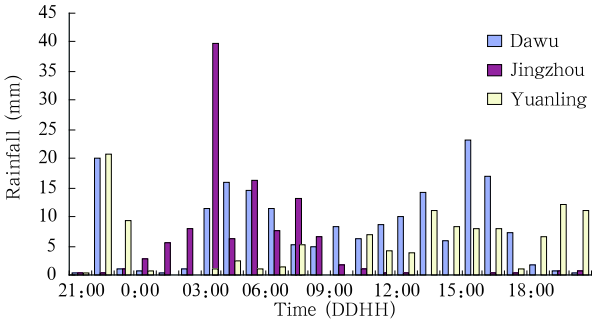

Fig.3. Hourly rainfall observed at Dawu, Jingzhou, and Yuanling in 24 h starting from 2000 BT 22 July 2002.

structure. In outside of SW-NE narrow rain band, there are several scattered rainfall centers in the middle of Henan Province, with 45-mm rainfall.

The intense observing rainfall data in six torrential rain centers of the rain band are available only at Dawu, Jingzhou, and Yuanling. The hourly rainfall (Fig.3) shows that there are different features in the three rainfall centers. There are three long-lasting rainfall peaks at Dawu and only a rainfall peak at Jingzhou with rainfall mainly in 0000-0800 BT and a maximum rain rate of 39.8 mm h^{-1} at 0300 BT 23 July. In contrast, the rainfall in Yuanling occurs before 0000 BT and after 0800 BT 23 July, with no rainfall in Jingzhou.

3. Mesoscale numerical model and initial value analysis system

3.1 *Mesoscale numerical model*

Advanced Regional Eta-coordinate Model (AREM) developed and improved by Yu et al. (1994;

2004) is used in this study. An η-vertical coordinate is designed in the model. The variables are distributed in E-horizontal grids, with a 37-km horizontal resolution, 28 vertical levels and 50-hPa model top. The model physics progresses include non-local PBL, horizontal diffusion, large scale rainfall condensation, Betts-Miller convective parameterized schemes, surface thermal balanced equation for temperature forecasting, energy budget for long and short wave radiation, surface sensible, and latent heat transportation. Moisture advection is calculated by advection difference. Lateral boundary is fixed. The model is integrated in a domain of 15°-55°N, 85°-135°E, with a grid of 0.5°(long.)×0.25°(lat.) and 150-s time step.

3.2 *Model initial value analysis system*

3.2.1 *Three-dimensional variational assimilation system*

A Grapes-3DVAR assimilation system (Zhang et al., 2004) developed by Numerical Forecasting Center of the Chinese Academy of Meteorological Sciences is used as the analysis system, which attributes the assimilation to a minimization of cost function:

$$\boldsymbol{J}(\boldsymbol{X}) = \frac{1}{2}(\boldsymbol{X}-\boldsymbol{X}^{\mathrm{b}})^{\mathrm{T}}\boldsymbol{B}^{-1}(\boldsymbol{X}-\boldsymbol{X}^{\mathrm{b}}) + \frac{1}{2}(\boldsymbol{H}(\boldsymbol{X})-\boldsymbol{y}^{\mathrm{o}})^{\mathrm{T}}\boldsymbol{O}^{-1}(\boldsymbol{H}(\boldsymbol{X})-\boldsymbol{y}^{\mathrm{o}}). \quad (1)$$

In this function, $\boldsymbol{X}$ is the analysis variable, $\boldsymbol{X}^{\mathrm{b}}$ is the background field, and $\boldsymbol{y}^{\mathrm{o}}$ is the observing field. $\boldsymbol{H}$ is an observing numerator, which is a mapping from model to observing space. $\boldsymbol{B}^{-1}$ is the inverse of covariance matrix of background errors. $\boldsymbol{O}^{-1}$ is the inverse of covariance matrix of observing errors. And T indicates matrix transposition.

Grapes-3DVAR is designed to be an A-grid horizontally and p-plane vertically. The cost function takes a form of incremental variable. Model variables are separated from analysis. The scheme adopts stream function, unbalanced potential velocity, unbalanced geopotential height, and humidity as analysis variables, which are independent of each other. The balanced restriction relationship of mass and wind field is also considered. To realize the computation of large ill-conditioned $\boldsymbol{B}^{-1}$, the background terms are preconditioned using a sequence of variable transformation, which improves convergence in minimization process, avoids the direct calculation of $\boldsymbol{B}^{-1}$, and decreases obviously the condition number of cost function's Hessian matrix. The relationship of physical variables, balanced restriction, EOF decomposition in vertical direction, and recursive filter in horizontal direction are used to realize three-dimensional variational assimilation. The LBFGS method is used in the optimization. Experiments show a reasonable relationship between the multi-variables and a fast convergence in the minimization process (see Zhang et al., 2004).

3.2.2 *Barnes objective analysis system*

Yu et al. (2004) designed an objective analysis scheme of meteorological fields—the improved Barnes objective analysis based on the principle of step-by-step correction method. The characteristics of the scheme are mainly as follows. They use global medium-range numerical forecast fields as the background, efficiently including meteorological information provided by four-dimensional global data assimilation and model forecast. Gauss distance weighted function is used as the weighted function of objective analysis, which makes analysis field contain more mesoscale features of weather systems. The interactive restriction relationship between wind and geopotential height can make wind and geopotential height analysis more consistent with each other. The calculation is accelerated due to station-centered scanning method. The advantage of Barnes method is that its weighted function is not related to the scanning radius threshold but only decided by scale response parameter K. Its basic feature can be decided by the analysis of response function. Its analysis iteration number decreases to two steps and no smoothing is needed in the analysis. The method is of low-passed-filter features and can be used to analyze different data.

3.2.3 *Barnes-3DVAR assimilation system*

On the basis of Barnes objective analysis and Grapes-3DVAR system, a new initial value analysis scheme, Barnes-3DVAR, is designed. The new scheme uses the assimilated analysis field from Grapes-3DVAR as background field and radiosoundings as

observational field. Then an optimal analysis field by Barnes method is used as model initial field.

4. Data and preprocess

The observational data used in this study include surface data, radiosoundings, reflectivities of Yichang, Changde and Jingzhou Doppler radars as well as Wuhan digital radar, radial velocities of Jingzhou and Yichang Doppler radars at 2000 BT 22 July 2002. Besides, the analysis fields of global medium-range numerical model T213L31 by the National Meteorological Center of China are used as initial background field of 3DVAR system. The horizontal resolution of T213L31 data is $1^\circ \times 1^\circ$ with 14 vertical levels (1000, 925, 850, 700, 600, 500, 400, 300, 250, 200, 150, 100, 70, and 50 hPa). The observed rainfall data include every 6-h observations from surface rain gauge and hourly intense rainfall observed by "973" Program (China Heavy Rain Program).

4.1 *Doppler-radar estimated 1-h rainfall*

S-wave Doppler radar at Yichang and Changde and C-wave portable Doppler radar at Jingzhou detected the rainfall systems with every 6-min volume scanning and obtained a large amount of detecting data. At first, echo intensity differences among three Doppler radars and Wuhan WSR-81S radar are compared within a detected rainfall cloud body. Then the reflectivities of four radars are corrected and 1-h surface rainfall is retrieved when mosaics are made. Last 1-h surface rainfall is obtained after four-radar retrieved rainfall mosaic is corrected by hourly rain gauge data with variational method (Zhang et al., 1992).

Rainfall data cannot be assimilated directly by Grapes-3DVAR so far. In the context of previous research, a rainfall assimilation scheme is designed. First, a one-dimensional variational assimilation system of rainfall developed by Wang et al. (2004a, b) is used to assimilate radar estimated 1-h rainfall and obtain optimal humidity profiles. Then the adjusted profiles are assimilated with Grapes-3DVAR system. Thus, the rainfall information is assimilated into initial model field.

4.2 *Doppler radar retrieved three-dimensional winds*

Radial velocities of only Jingzhou and Yichang Doppler radars in this heavy rain are obtained. Before three-dimensional variational assimilation, radial velocities detected by Jingzhou and Yichang Doppler radars at 2000 BT 22 July 2002 are first retrieved to get three-dimensional winds at different levels with VVP method, horizontal and vertical resolutions of which are both 1 km in a range of 120-km scanning radius. The retrieved winds at different levels and radial velocities are compared and shown to be very consistent, which indicate that the retrieved horizontal winds can basically reflect mean features of real environmental winds. Cheng et al. (2004) compared winds retrieved from dual Doppler radar and those from single Doppler radar by VVP method and simple conjugate method, and found that the retrieved winds can both reflect wind structure and its evolution although these methods are different.

The three-dimensional retrieved wind vectors u, v, and w by improved VVP method (Wei, 1998) are obtained at the same height level in radar rectangular coordinate. But the winds to be assimilated by Grapes-3DVAR system should be in latitude and longitude coordinates at isobaric surface. Therefore, the retrieved winds are needed to carry out coordinate transformation. First, the radar rectangular coordinate is changed into latitude and longitude coordinates (Wan et al., 1990). Then according to the height of retrieved winds and the height and pressure of radiosounding, horizontal winds under latitude and longitude coordinates at isobaric surface are obtained by dual linear interpolation. The vectors in Figs.4a, b are retrieved horizontal wind vectors at 700 hPa from Yichang and Jingzhou Doppler radars (some data are omitted for clearance in drawing the figure). Wind barb is radiosoundings. There are only two radiosounding stations (Wuhan and Yichang) in the figure domain. Figure 4 shows that horizontal winds retrieved from Wuhan and Yichang Doppler radars are in a good consistency with radiosoundings at 700 hPa

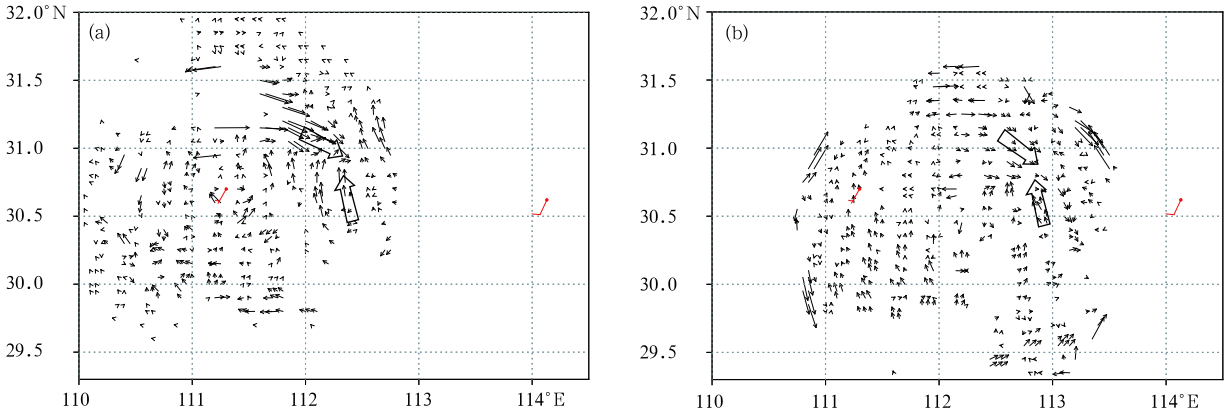

Fig.4. 700-hPa winds retrieved from the Yichang (a) and Jingzhou (b) Doppler radar data (vectors) and observed by radiosoundings (barbed arrows) at 2000 BT 22 July 2002.

in wind direction and velocity, and single radar retrieved winds are also basically consistent with radiosoundings in the two-radar covering area. This indicates that the horizontal winds retrieved by VVP method can reflect wind basic structure. But radar retrieved horizontal winds contain fine mesoscale wind information which cannot be provided by radiosoundings. For example, there is an obvious east-west directed wind discontinuity line−shear line in Jianghan Plain area of Hubei Province.

5. 3DVAR numerical experiments

5.1 *Experimental design*

Convergence and moisture at lower levels are very important for rainfall formation and evolution. In order to investigate independent roles of Doppler radar rainfall or wind assimilation and their interaction, three dimensional variational assimilation experiments are designed as follows (Table 1).

Table 1. Assimilation schemes for Doppler-radar-estimated precipitation radar and radar-retrieved winds

Initialization Scheme	Experiment name	Observing field	Background field
Grapes-3DVAR	TK	Soundings	T213L31 analysis field
	RH	Soundings+radar-estimated rainfall	
	RW	Soundings+radar-retrieved winds	
	RH&RW	Soundings + radar-estimated rainfall+ radar-retrieved winds	
Barnes	B-T213	Soundings	T213L31 analysis field
Barnes-3DVAR	B-TK	Soundings	Experiment TK analysis field
	B-RH		Experiment RH analysis field
	B-RW		Experiment RW analysis field
	B-RH&RW		Experiment RH&RW analysis field

The Grapes-3DVAR system is used as initialization scheme. Four experiments are designed on the basis of observation data types: (1) radiosoundings (Exp.TK), (2) radiosoundings and Doppler radar estimated rainfall (Exp.RH), (3) radiosoundings and Doppler radar retrieved winds (Exp.RW), and (4) radiosoundings, Doppler radar estimated rainfall and retrieved winds (Exp.RH&RW) at 2000 BT 22 July. The background fields of the four experiments are T213L31 model analysis field at 2000 BT 22 July.

5.2 *24-h rainfall forecast analysis*

Figure 5 is the simulated 24-h rainfall starting from 2000 BT 22 July with analysis field of different observing data assimilations as model initial field. It can be seen that Exp.TK simulates a narrow rain band

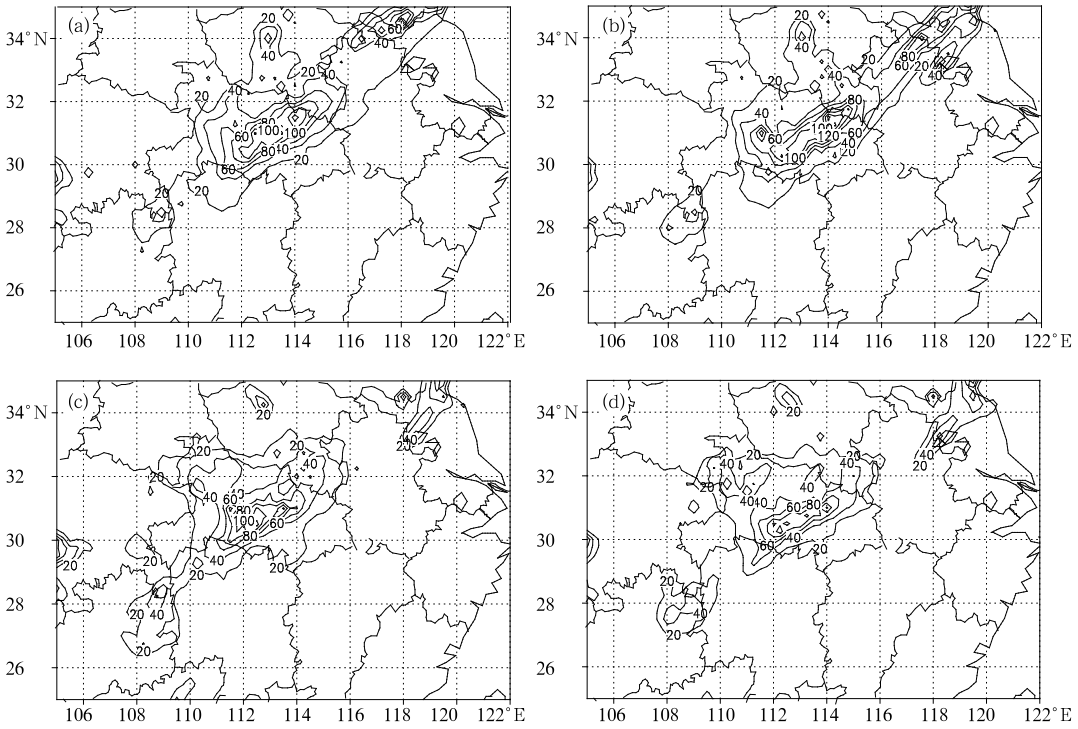

Fig.5. Rainfall (unit: mm) simulated in the three-dimensional variational assimilation experiments of TK (a), RH (b), RW (c), and RH&RW (d) in 24 h starting from 2000 BT 22 July 2002.

oriented NE-SW in the connecting area of Hubei, Henan, Anhui, Jiangsu, and Shandong Provinces with intense rainfall concentrated in the east of Hubei and the south of Shandong (Fig.5a). As compared with observations, the deficiency of 24-h rainfall simulation by Exp.TK is: (1) The simulated rain band is obviously weak with 20-mm isohyet only at 28°N, 108°E and the above 20-mm rain band is not continuous in the connecting area of Guizhou-Hunan and Hubei-Hunan Provinces. But the observed 20-mm isohyet crosses Jiangsu, Anhui, Hubei, Hunan, and Guizhou, being a continuous rain band. (2) The simulated rainfall center is obviously weak, with the rainfall centers of simulated rain band mainly in the east of Hubei, the connecting area of Jiangsu-Henan-Anhui, the center of Henan and the connecting area of Guizhou-Sichuan-Hunan. Although the location and intensity are different when compared with observations, the three rainfall centers in the center of Henan and the connecting area of Jiangsu-Henan-Anhui are simulated relatively well. Furthermore, model simulates the rainfall center at Dawu and Jingzhou successfully. The location of rainfall center at Dawu is simulated well although its 132-mm intensity is a little weaker (observation is 192.4 mm). The deficiency lies in the simulation of the rain band in Guizhou and the connecting area of Hubei-Hunan. (3) The location of simulated rain band is different from observations, with its location further northeast than observation, that is, the longitude of simulated rain band is larger than observation.

Figure 5b shows the rainfall simulations of EXP. RH. It can be seen that, after the assimilation of radar estimated rainfall information into model initial field, the difference of simulated rain band shape, location and orientation between Exp.TK and Exp.RH is very little. But Exp.RH improves the simulation of rainfall center structure and intensity. First the simulated rainfall near Dawu increases from 132 to 151 mm. Secondly, the simulated mesoscale rain mass in Hubei is clearer. Thirdly, the simulated rain mass in the connecting area of Jiangsu-Anhui are more close to observation. The observations indicate there are four rainfall centers, which are located in Bengbu, Suqian, Huaiyin, and Sheyang, respectively. The maximum

rainfall center is in Bengbu with a rainfall intensity of 128 mm near 32.95°N, 117.38°E. Exp.TK simulated out three rainfall centers with maximum rainfall center located in 34.5°N, 118°E (148 mm). Exp.RH simulated four rainfall centers with maximum rainfall center located in 34°N, 117.5°E (112 mm). The rainfall center intensity and location are closer to observations. Consequently the assimilation of radar rainfall in Exp.RH on the basis of Exp.TK exerts a positive effect on the 24-h rainfall simulation.

Figure 5c is the simulated rainfall by Exp.RW. It can be shown that, when comparing Exps.TK and RW, the distribution of rainfall band is changed and rainfall is not in a shape of band. The rainfall in Hubei and the connecting area of Jiangsu-Anhui is not simulated well. It should be paid attention to that there are some improvements although the simulation of rain band is a little worse on the whole after radar retrieved winds assimilated into initial field. First, Exp.RW simulated a single rain mass in the central Henan, which is connected with the main rain band in Exps.TK and RH and stronger than observation. Secondly, the rainfall simulation in the connecting area of Guizhou and Hunan is improved, that is, rainfall intensity is increased.

Figure 5d shows the rainfall simulation of Exp. RH&RW. The simulation is the worst are when compared with above-mentioned experiments. The main rain band is broken up into three parts and the rainfall intensity is obviously weaker.

5.3 *Analysis of 6-h rainfall forecast differences*

The effects of assimilation of radar-estimated rainfall and radar-retrieved winds on the rainfall forecast can be understood when taking Exp.TK as control experiment to investigate the rainfall forecast differences between Exps.RH, RW, and RH&RW in different times.

After the investigation of rainfall difference fields in the four periods of 0-6, 6-12, 12-18, and 18-24 h, it can be found that:

(1) The 6-h rainfall forecasts are influenced obviously in Grapes-3DVAR scheme no matter assimilating the estimated precipitation or retrieved winds respectively, or both of them. The 18-24 h simulated rainfall differences of Exps.RH, RW, and RH&RW are -50−60, -80−30, and -90−40 mm, which indicate that the assimilation of radar-estimated rainfall and radar-retrieved winds still affect 18-24-h rainfall forecast.

(2) In Grapes-3DVAR scheme, the effects of Exps.RH and RW on 6-h precipitation are different in initial model integration, but later the effects come to be the same with model integration.

6. Numerical experiments of Barnes objective analysis

6.1 *Experimental design*

The designed experimental scheme B-T213 is as follows (Table 1). The initial value is generated by Barnes objective analysis method, with radiosoundings as observational field and T213L31 analysis as background field at 2000 BT 22 July. It can be found that, when comparing Exp.B-T213 with Exp.TK, the data used in the experiments are totally same. The different point is that Exp.B-T213 uses Barnes objective analysis method as initial value scheme, while Exp.TK uses Grapes-3DVAR scheme.

6.2 *Analysis of 24-h rainfall forecast*

Figure 6 gives the 24-h simulated rainfall of Exp.B-T213. It is shown that the model simulates a narrow NE-SW rain band across Jiangsu, Anhui, Hunan, and Guizhou, and the simulated maximum intensity center is near Dawu with rainfall of 225 mm, which is very close to the observation. On the whole, Barnes scheme successfully simulated the whole rain band, the shape, location, and intensity of which are all close to observations. It can be found that, when the details of the rain band are analyzed, Barnes scheme has some deficiencies in rain band simulation: (1) the whole rain band is a little further north than observation, (2) there exist rainfall differences in the connecting area of Jiangsu-Anhui between the simulation and observation, with some rainfall centers not simulated, and (3) the rain mass in central Henan is not simulated. When compared with Exp.TK, it indicates that the 3DVAR scheme simulates well in the above aspects: the location of simulated rain band in Exp.TK is consistent with observation and the rainfall center in the central

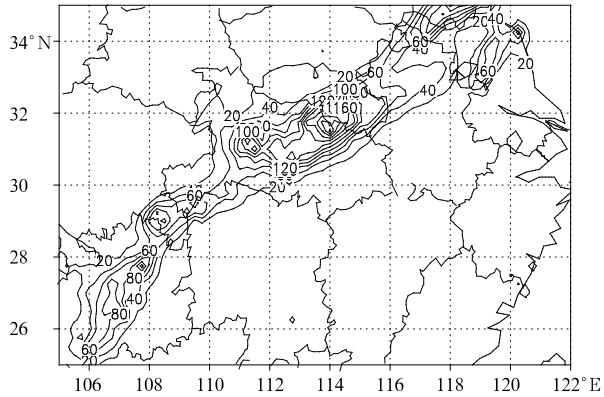

Fig.6. Rainfall (unit: mm) simulated in 24 h starting from 2000 BT 22 July 2002 in Exp.B-T213.

Henan is simulated out. Also the rainfall centers in the connecting area of Jiangsu-Anhui is simulated successfully with mesoscale rain mass simulated well. But Exp.TK does not simulate the whole rain band.

It can be seen that Barnes scheme and 3DVAR scheme have their own advantages and disadvantages. For this heavy rain case, Barnes scheme simulates better on the whole, which reflects that AREM model has the capability to simulate wide-range heavy rainfall. Since the two schemes have their advantages and disadvantages respectively, can we design a new initial value scheme, which can include Barnes scheme and 3DVAR?

7. Numerical experiments of Barnes-3DVAR scheme

7.1 *Experimental design*

In Barnes-3DVAR scheme, the analysis field obtained from the assimilation of Grapes-3DVAR system is taken as background field, radiosoundings are used as observed field, and the optimized analysis field obtained by Barnes method is adopted as model initial field. According to different background fields, experiments are further divided into four types (Table 1): 1) Exp.B-TK, taking the analysis field of Exp.TK as the background field; 2) Exp.B-RH, taking the analysis field of Exp.RH as the background field; 3) Exp.B-RW, taking the analysis field of Exp.RW as the background field; and 4) Exp.B-RH&RW, taking the analysis field of Exp.RH&RW as the background field. In the four experiments, the radiosoundings at 2000 BT 22 July are used as the observed field. Compared with Barnes scheme, the advantage of Barnes-3DVAR scheme is that, with the help of Grapes-3DVAR system, non-routine observational data such as radar detections can be assimilated into model initial field.

7.2 *24-h simulated precipitation analysis*

The 24-h simulated precipitation starting at 2000 BT 22 July is shown in Fig.7, with the analysis field obtained from assimilation of different kinds of observations as model initial field at 2000 BT 22 July. Comparing EXP.B-TK (Fig.7a) with Exp.B-T213 (Fig.6), we can see, although the same data are used, the simulated rain belts have changed due to the reason that different initialization schemes are used to generate model initial field. In Barnes-3DVAR scheme, rainfall distribution and location are so obviously improved that they are consistent with observations. Comparing Exp.TK (Fig.5a), Exp.B-T213 (Fig.6), and Exp.B-TK (Fig.7a), it is indicated that the simulations of rain belts are very different in the three different initialization schemes although the same radiosoundings and T213L31 analysis field are used. In Grapes-3DVAR scheme, the rain belt is incompletely simulated, but some mesoscale can be depicted in detail. In Barnes scheme, the rain band is completely simulated, but it slightly slants to the north. In Barnes-3DVAR scheme, the rain belt is completely simulated and its location corresponds with observation.

With Barnes-3DVAR scheme, Exp.B-RH (Fig.7b) in which radar retrieved precipitation and radiosoundings are assimilated into model initial field shows that rain belt is simulated very well, its location corresponds with observation, and rain band mesoscale details are obviously reflected. Three rainfall centers near the common boundary areas of Jiangsu and Anhui, rainfall center at Bengbu, and rainfall center in Northwest Hunan are well simulated.

Different from Exps.RW and RW&RH in Grapes-3DVAR schemes, Exps.B-RW and B-RW&RH in Barnes-3DVAR scheme successfully simulate the rain belt. Compared with the tests where only

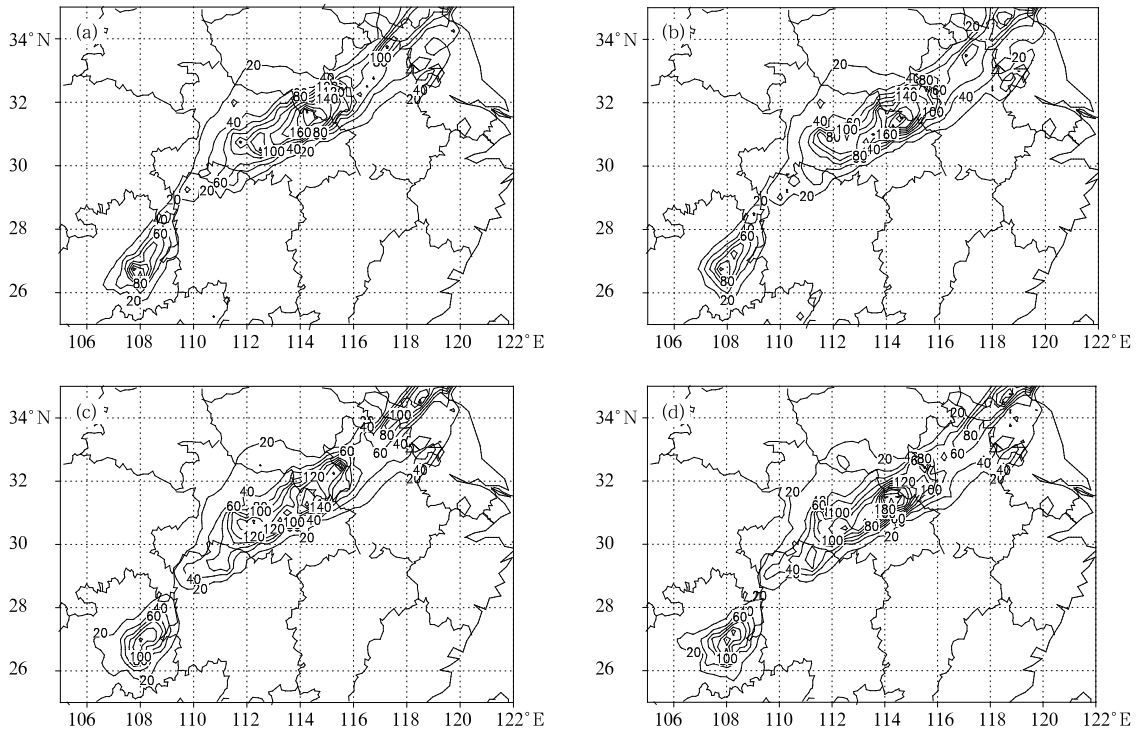

Fig.7. Rainfall (unit: mm) simulated in 24 h starting from 2000 BT 22 July 2002 in the Barnes-3DVAR assimilation experiments of B-TK (a), B-RH (b), B-RW (c), and B-RH&RW (d).

radiosounding data are assimilated, the simulated rainfall intensity and location are further close to observations. Exp.B-RW&RH does not only simulate rain band location, but also precipitation centers (except rainfall at Yuanling), which are close to observations in intensity and location.

7.3 *Analysis of 6-h precipitation forecast differences*

Taking Exp.B-TK as control experiment, 6-h precipitation forecasting differences among Exps.B-TK, B-RH, B-RW, and B-RH&RW are respectively studied in order to find out the effects of radar retrieved precipitation and wind assimilation on rainfall forecast in Barnes-3DVAR scheme. The results are as follows.

(1) Under Barnes-3DVAR scheme, 6-h precipitation fields are obviously affected no matter assimilating the estimated precipitation or retrieved winds or both of them. In Exps.B-RH, B-RW, and B-RH&RW, 18-24-h precipitation differences are from −40 to 15 mm, from −30 to 60 mm, and from −25 to 40 mm, respectively, which indicates that radar estimated precipitation and retrieved wind assimilation can obviously affect 18-24-h precipitation forecast.

(2) Under Barnes-3DVAR scheme, radar-retrieved wind assimilation affects precipitation field more strongly than radar-estimated precipitation does. More positive or negative centers of 6-h precipitation differences appear in Exp.B-RW and their intensities are much stronger than those in Exp.B-RH (Figs.8a, b). So do differences of 0-6-, 6-12-, 12-18-, and 18-24-h simulated precipitation.

(3) Different from Grapes-3DVAR scheme, the effect of Barnes-3DVAR scheme on precipitation forecast is consistent when radar estimated precipitation and retrieved winds are respectively or simultaneously assimilated (Fig.8). The same negative or positive centers of precipitation differences in Exp.B-RH appear at the same positions as in Exps.B-RW and B-RH&RW. It is very significant that the differences of 0-6-, 6-12-, 12-18-, and 18-24-h precipitation are all in this way. These facts show that Barnes-3DVAR is superior to Grapes-3DVAR scheme.

(4) The simultaneous assimilation of radar

retrieved precipitation and wind does not mean adding them simply together. As it is shown in Figs.8a, b, when only precipitation or only wind is assimilated, the positive difference center appears at Dawu in 6-12-h model integration, with small range and weak intensity (10 mm). When retrieved precipitation and wind are both assimilated, the difference at Dawu is 50 mm (Fig.8c). The evolution of observed hourly rainfall at Dawu (Fig.3) shows that the second rainfall peak took place in 6-12 model hours, i.e., at 0200 to 0800 BT 23 July 2002.

In this paper, Barnes-3DVAR scheme, which includes the advantages of Grapes-3DVAR and Barnes objective analysis method, is a new kind of initialization scheme in which radar estimated precipitation and retrieved winds can be assimilated. It can simulate precipitation better than Grapes-3DVAR scheme. The torrential rain in the Middle Reaches of the Yangtze River from 0800 BT 8 July to 0800 BT 9 July is also examined. The result shows that the model successfully simulates 24-h precipitation after Doppler radar detections at Wuhan and Yichang are assimilated in Grapes-3DVAR scheme. But in Barnes-3DVAR scheme, the model simulates 24-h precipitation better than in Grapes-3DVAR scheme after radar retrieved winds are assimilated. This indicates that precipitation forecasting is better after Barnes-3DVAR scheme has adjusted Grapes-3DVAR analysis field.

8. Effect of Grapes-3DVAR and Barnes-3DVAR on element field

The same radiosoundings and T213L31 model analysis field are used in Exps.TK and B-TK. However, Grapes-3DVAR scheme is used in Exp.TK while Barnes-3DVAR scheme is adopted in Exp.B-TK. The 24-h precipitation simulation in Exp.B-TK is much better than that in Exp.TK. What are the differences between the two experiments in element field simulation?

Firstly, the distribution of wind, geopotential height, temperature, and vapor field at initial time (2000 BT 22 July 2002) at different isobaric surfaces is studied. As is shown in the 700-hPa wind distribution, flow field structure is similar in the two

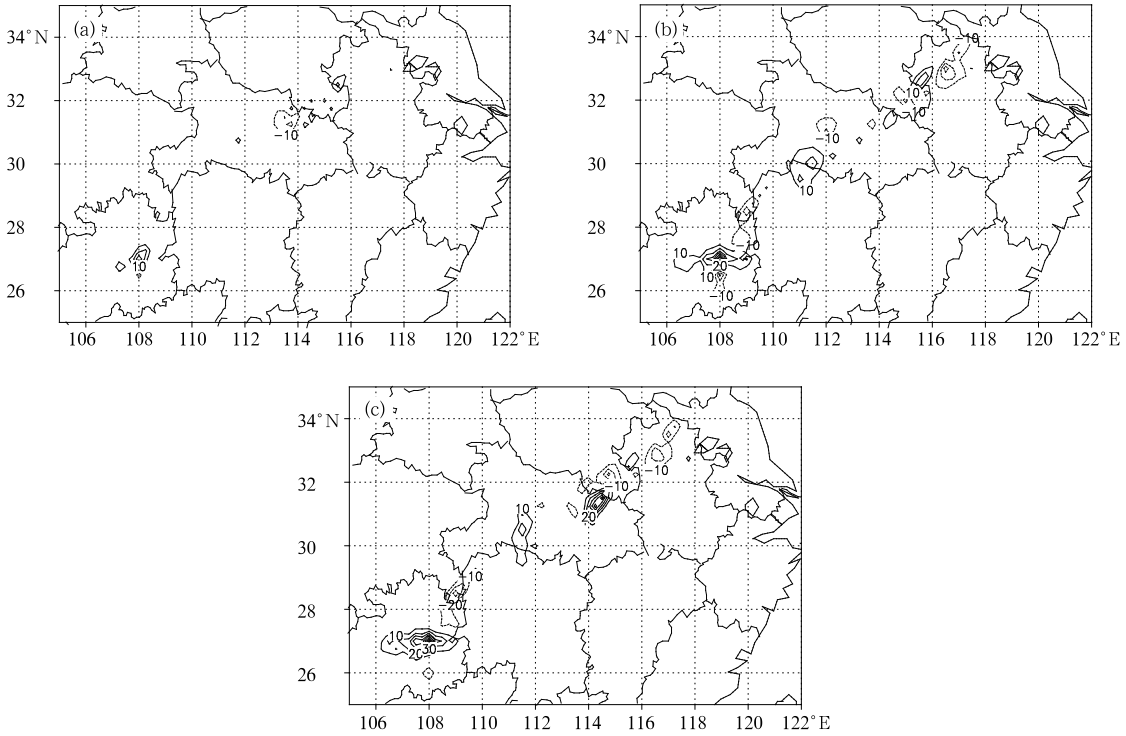

Fig.8. Simulated rainfall differences (unit: mm) of Exp.B-TK with Exp.B-RH (a), Exp.B-RW (b), and Exp.B-RH&RW (c) in the period of 6-12-h model integration.

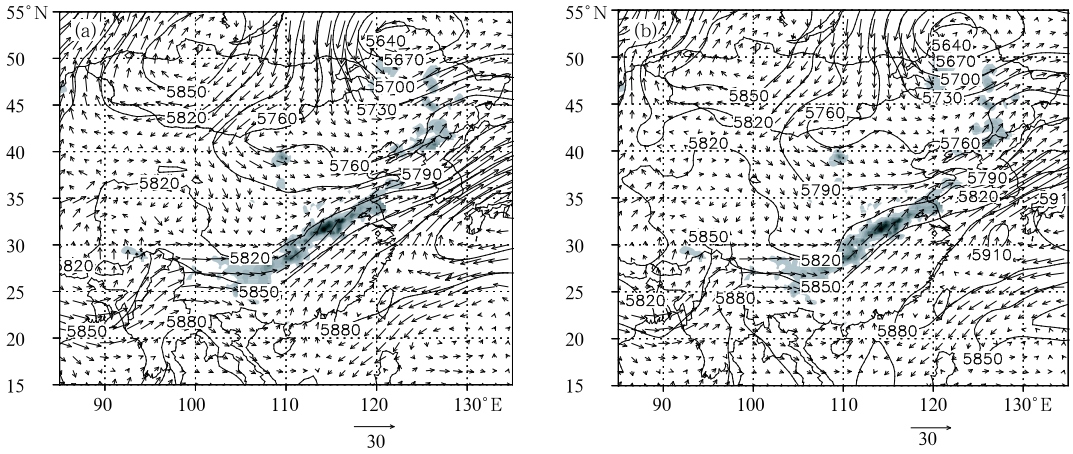

Fig.9. Geopotential height (unit: gpm) and wind fields (unit: m s^{-1}) at 500 hPa in Exp.TK (a) and Exp.B-TK (b) at 2000 BT 22 July 2002, with the shading area indicating the observed 24-h rainfall.

experiments. There are three closed cyclonic circulations to the north side of rain belt and a wide and strong anticyclonic circulation to its south side. The rain belt lies just in southwest warm and moist air to the south side of 700-hPa shear line. As is shown in 500-hPa situation field, 500-hPa circulation at high latitude areas of Europe and Asia also presents a pattern of "two troughs and one ridge" in the two experiments. There is a low trough to the east side of Ural Mountains and another low trough in North China. The high ridge at Baikal Lake shows a blocking pattern. The western Pacific subtropical high is oriented in northwest and southwest. The main differences between 500-hPa analysis fields in the two experiments are that the high at Baikal Lake is strengthened and the low vortex at Northeast China is deepened in Exp.B-TK. Besides, the simulated West Pacific subtropical high is different in the two experiments. Especially in the south of the subtropical high, Exp.TK simulates a cyclonic circulation in wind fields, which is not reflected in height field. But Exp.B-TK (Fig.9) simulates a closed low in the area of cyclonic circulation. When viewed from 850-hPa specific humidity and temperature differences, there exist positive specific humidity and temperature differences along the rain band. The biggest specific humidity increment is 1.5 g kg^{-1} and the biggest temperature increment is 1.5°C (Fig.10a). On the cross section along 114°E (heavy rain center at Dawu), the positive specific humidity difference concentrates in heavy rain area from lower level to 600 hPa with the positive temperature differences at 900-200 hPa. Above analysis shows that model initial field has changed after analysis field obtained from Grapes-3DVAR scheme (Exp.TK) is analyzed by Barnes objective analysis method (Exp.B-TK). That is, the upper air above the surface rain band becomes moister and warmer, and the 500-hPa blocking high at middle and high latitudes becomes stronger.

In the following, the hourly evolutions of element fields in Exps.TK and B-TK are examined respectively and it is found that the 500-hPa blocking high in East Asia, the cold vortex in North China and the subtropical high are stable continuously. In order to find out the reasons for the simulated rainfall differences of the two experiments, their wind- and height-mean fields are shown in Fig.11. There are obvious differences between them. In Exp.B-TK, the Baikal Lake blocking high is wide and strong. The West Pacific subtropical high extends to west further than in Exp.TK and its west ridge point reaches 115.5°E. But in Exp.TK, the ridge point reaches 120.5°E. In Exp.TK (Fig.11a), there exist two trough lines at 500 hPa in the east of China. One is North China low trough, whose bottom is located at 35°N, 110°E. Due to the Middle and Lower Reaches of the Yangtze River to the east of 110°E just locating in the front of North China low trough, Exp.TK successfully simulates the rain band

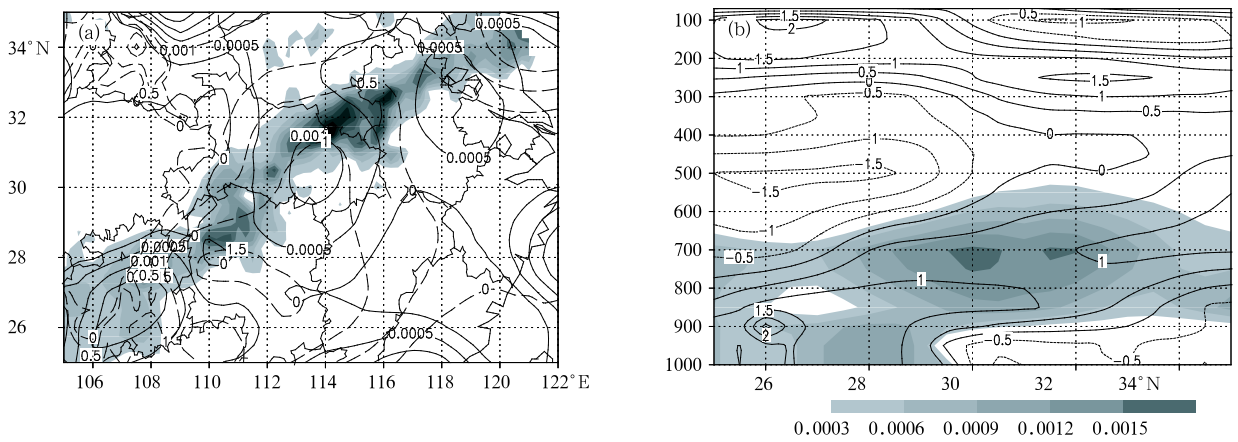

Fig.10. Differences of specific humidity (solid line, unit: kg kg^{-1}) and temperature (dashed line, unit: °C) between Exps.B-TK and TK (Exp.B-TK minus Exp.TK) at 850 hPa at 2000 BT 22 July 2002 (a, the shading indicates the 24-h observed rainfall), and their vertical cross section along 114°E (b).

to the east of 110°E. But the intensity of precipitation center is not fully simulated because it is a little far away from the trough line. The second trough line locates near 108°E and orients from south to north, so the model simulates out the precipitation at areas between 108° and 110°E, but the precipitation in Guizhou and other provinces to the west of 108°E (Fig.5a) is not simulated out because it lies in the behind of southern trough. In Exp.B-TK, the locations of the vortex and the trough have obviously changed because the Baikal Lake blocking high is strengthened and the West Pacific subtropical high extends westward. Under this synoptic pattern, the location of upper trough is obviously different from that in Exp.TK. In Exp.B-TK, there is only a 3000-km upper trough oriented in NE-SW, stretching from (50°N, 122°E) to (27°N, 110°E). The 24-h observed rainfall in Northeast China and the reaches of the Yangtze River just takes place in the southwest flow in front of upper trough. Moreover, the observed rain band is very near the trough line. The whole rain band is completely simulated out in Exp.B-TK and its intensity is also close to observations.

In Exp.TK, the analysis field obtained by assimilating radiosoundings with Grapes-3DVAR scheme is used as model initial field. Because there exist differences between initial temperature, pressure, moisture and wind fields, and corresponding observations, the differences further increase in the model integration so that the simulated precipitation is totally different from observation. But in Exp.B-TK, the analysis field of Exp.TK is used as background field and it is combined with radiosoundings together by Barnes objective analysis method, i.e., the analysis field of Grapes-3DVAR improved by Barnes objective analysis method is used as model initial field. The analysis indicates that, due to the adjustments of the Baikal Lake blocking high, West Pacific subtropical high, and other element fields under Grapes-3DVAR scheme at initial time, the synoptic pattern is very favorable for the occurrence of close-to-observation rainfall.

When comparing another group of experiments, Exps.RH&RW with B-RH&RW, where the same data sources (radiosoundings, radar estimated precipitation, retrieved winds, and T213L31 analysis fields) are used, the results are very similar to comparison analysis of Exps.TK and B-TK. In Exp.RH&RW of Grapes-3DVAR scheme, the upper air trough line location is not favorable for close-to-real rainfall forecast due to small range and weakness of the Baikal Lake blocking high and the West Pacific subtropical high extending eastward to 123°E. However in Exp.B-RH&RW, after the analysis field of Grapes-3DVAR has been adjusted by Barnes objective analysis method, the Baikal Lake blocking high is strengthened and the subtropical high extends westward. The upper air trough location is favorable for close-to-real rainfall forecast.

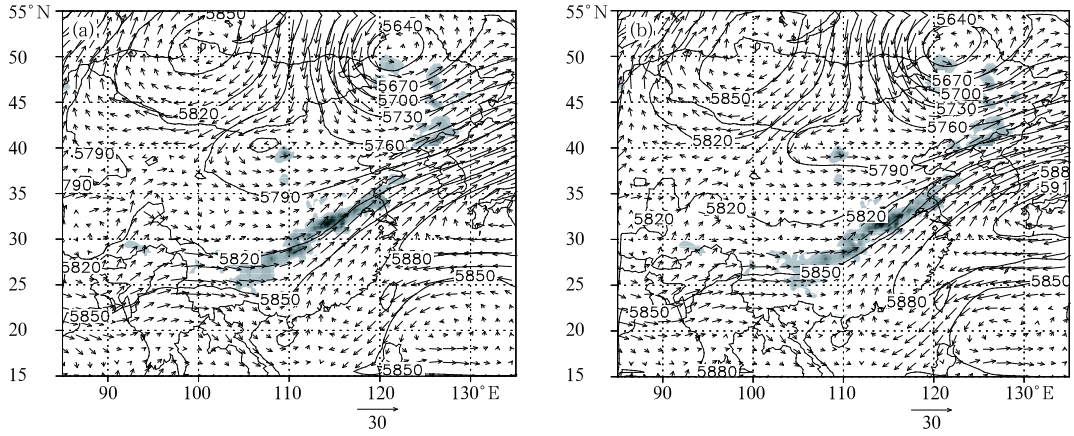

Fig.11. Mean geopotential height (units: gpm) and wind fields (units: m s^{-1}) at 500 hPa over the 24 h starting from 2000 BT 22 July 2002 simulated in Exp.TK (a) and Exp.B-TK (b) (the shading indicates the observed 24-h rainfall).

9. Concluding remarks

On the basis of the joint estimated 1-h precipitation from Changde, Jingzhou, and Yichang Doppler radars as well as Wuhan digital weather radar, and the retrieved wind fields from Yichang and Jingzhou Doppler radars, a set of numerical experiments under different model initial schemes with an advanced regional η-coordinate model (AREM), i.e., Grapes-3DVAR, Barnes objective analysis and Barnes-3DVAR, are carried out to simulate a heavy rain in 24-h period starting at 2000 BT 22 July 2002 along the Yangtze River and investigate the effects of the Doppler radar estimated rainfall and retrieved winds on the rainfall forecast. The main results are as follows:

(1) The simulations are obviously different under three initial schemes with the same data source (radiosoundings and T213L31 analysis). On the whole, Barnes-3DVAR, which combines the advantages of Barnes objective analysis and Grapes-3DVAR method, gives the best simulations: well-simulated rain band and clear mesoscale structures, as well as their location and intensity close to observations.

(2) Both Barnes-3DVAR and Grapes-3DVAR schemes are able to assimilate Doppler radar estimated rainfall and retrieved winds, but the differences in simulation results are very large. Barnes-3DVAR's simulation is much better than Grapes-3DVAR's.

(3) Under Grapes-3DVAR scheme, the simulation of 24-h rainfall is improved obviously when assimilating Doppler radar estimated precipitation into model in comparison with control experiment. But it becomes a little worse when assimilating Doppler radar retrieved winds into model, and it becomes worse when assimilating Doppler radar estimated precipitation as well as retrieved winds into model. However, the simulation is different under Barnes-3DVAR scheme. The simulation is improved to a certain degree no matter assimilating the estimated precipitation or retrieved winds, respectively, or both of them. The result is the best when assimilating both of them into model—the orientation and location of simulated rain band is close to observation, rainfall centers on the rain band, except one near Yuanling, are simulated out and well close to real case and rainfall intensity is also basically consistent with the observation.

(4) The assimilation of radar estimated precipitation and retrieved winds even has an obvious effect on 18-24-h rainfall simulations. Under Barnes-3DVAR scheme, the effects on rainfall forecast are consistent no matter assimilating the estimated precipitation or retrieved winds, or both of them. The simultaneous assimilation of retrieved winds and estimated precipitation exerts a most obvious influence on rainfall simulation. The radar retrieved wind assimilation comes

to the second and the radar estimated precipitation assimilation comes to the last.

(5) Under Grapes-3DVAR scheme, because the simulated Baikal Lake blocking high is relatively weak, the West Pacific subtropical high extends eastward and the vapor is not enough in heavy rain area, the simulation is not so successful. Under Barnes-3DVAR scheme, the simulated rain belt is more close to real situation after the analysis field of Grapes-3DVAR has been adjusted, because the Baikal Lake blocking high is strengthened, the West Pacific subtropical high extends westward and the air in heavy rain area becomes warmer and moister.

(6) Under Grapes-3DVAR scheme, the simulation can be improved when the radar estimated precipitation and retrieved winds are assimilated respectively. But when the two are simultaneously assimilated into model initial field, the rainfall forecasting becomes poor obviously. Is it due to the poor compatibility of the two kinds of data or some non-consistency in Grapes-3DVAR assimilation of the two kinds of data? Or is it because, when compared with the background field, the dense wind field retrieved by VVP method is so "scattered" that it is regarded as "noise" and negatively affects the analysis field? This problem remains to be studied in the future. But when the analysis field obtained by assimilating radar estimated precipitation and retrieved winds with Grapes-3DVAR system is used as the background field and the analysis field obtained by analyzing soundings with Barnes objective analysis method is used as the initial field, the model forecasting is very successful. This indicates that radar estimated precipitation and retrieved winds should be very significant to describe mesoscale details and that the critical points is how to assimilate them into model initial field reasonably. The Barnes-3DVAR scheme designed in this paper is no doubt a new kind of method to apply these kinds of data.

REFERENCES

Cheng Minghu, Liu Liping, Zhang Peiyuan, et al., 2004: *Principle and techniques of heavy rainfall retrieval using Doppler radar data.* China Meteorological Press, Beijing, 254 pp. (in Chinese)

Gal-Chen, T., 1978: A method for the initialization of the anelastic equations: Implication for matching models with observations. *Mon. Wea. Rev.*, **106**, 587-606.

Gao, J., Xue M., Wang Z., et al., 1998: The initial condition and explicit prediction of convection using ARPS adjoint and other retrieval methods with WSR-88D data. AZ, Amer. Meteor. Soc., 176-178.

Qiu, C., and Xu Q., 1992: A simple adjoint method of wind analysis for single-Doppler radar data. *J. Atmos. Oceanic Tech.*, **9**, 588-598.

Qiu Chongjian, Yu Jinxiang, and Qin Xu, 2000: Use of Doppler-radar data in improving short-term prediction of mesoscale weather. *Acta Meteor. Sinica*, **58**(2), 244-249. (in Chinese)

Ma Qingyun, Li Zechun, and Tao Shiwei, 2001: Wind-field retrieval through single Doppler weather radar and its application to NWP. *Quart. J. Appl. Meteor.*, **12**(4), 488-493. (in Chinese)

Sun, J., D. Flicher, and D. Lilly, 1991: Recovery of three-dimensional wind and temperature fields from single-Doppler radar data. *J. Atmos. Sci.*, **48**, 876-890.

Shapiro, A. S. Ellis, and J. Shaw, 1995: Single-Doppler velocity retrievals with Phoenix data: Clear air and microburst wind retrievals in the planetary boundary layer. *J. Atmos. Sci.*, **52**, 1265-1287.

Shapiro, A. et al., 1996: Initial forecast fields created from single-Doppler wind retrieval, thermodynamic retrieval and ADAS. Preprint. 11th Conf. on NWP, American Meteorological Society. 5A.7

Sun, J. et al., 1991: Recovery of three-dimensional wind and temperature fields from single-Doppler radar data. *J. Atmos. Sci.*, **48**, 876-890.

Sun, J., and N. Crook, 1994: Wind and thermodynamic retrieval from single-Doppler measurements of a gust front observed during Phoenix II. *Mon. Wea. Rev.*, **122**, 1075-1091.

Sun, J., and N. Crook, 1997: Dynamical and microphysical retrieval from Doppler radar observations using a cloud and its adjoint. Part I: Model development and simulated data experiments. *J. Atmos. Sci.*, **54**, 1642-1661.

Sun, J., and N. Crook, 1998: Dynamical and microphysical retrieval from Doppler radar observations using a cloud and its adjoint. Part II: Retrieval experiments of an observed Florida convective storm. *J. Atmos. Sci.*, **55**, 835-852.

Shi Wangzhi, Jin Qi, and Guo Shi, 2003: Diagnostic analysis of a continuous heavy rain event in Hubei. *Meteor. J. of Hubei*, (4), 7-9. (in Chinese)

Tao Shiyan, 1980: *Torrential Rain in China*. Science Press, Beijing, 225 pp. (in Chinese)

Tao Zuyu, 1992: The VAP method to retrieve the wind vector field based on single-Doppler velocity field. *Acta Meteor. Sinica*, **50**(1), 81-90. (in Chinese)

Weygandt, S., 1998: The retrieval of initial forecast fields from single-Doppler observations of a supercell thunderstorm. Ph. D. dissertation, University of Oklahoma, 257 pp.

Wang Yehong, Zhao Yuchun, and Cui Chunguang, 2004a: Sensitivity research on one-dimensional variational assimilation of radar-derived precipitation. *Meteor. Monthly*, **30**(4), 6-10. (in Chinese)

Wang Yehong, Cui Chunguang, and Zhao Yuchun, 2004b: One-dimensional variational assimilation of radar-derived precipitation data: retrieving of humidity. *Meteorological Science and Technology*, **32**(5), 322-328. (in Chinese)

Wan Qilin, Xue Jishan, and Zhuang Shiyu, 2005: Study on the variational assimilation technique for the retrieval of wind fields from Doppler radar data. *Acta Meteor. Sinica*, **63**(2), 129-145. (in Chinese)

Wei Ming, 1998: Three-dimensional wind field retrieving from a single Doppler radar data with VVP method (dissertation). Nanjing University, Nanjing. (in Chinese)

Wan Yufa, Chen Shaolin, Luo Jianguo, et al., 1990: Coordinate assimilation of radar and satellite imagery and its implementation. *J. Nanjing Insti. Meteor.*, **13**(4), 638-643. (in Chinese)

Xiao Yanjiao, Zhang Jiaguo, Wan Rong, et al., 2005: Mesoanalysis of shear line heavy rain with Doppler radar observations. *Meteor. Monthly*, **31**(2), 35-37. (in Chinese)

Yu Rucong, 1994: A test for numerical weather prediction of real-time for China flood season precipitation in 1993 by a regional η-coordinate model. *Chinese J. Atmos. Sci.*, **18**(3), 284-292. (in Chinese)

Yu Rucong, Xue Jishan, Xu Youping, et al., 2004: *An advanced regional Eta-coordinate numerical heavy-rain prediction model (AREM) system (AREMS).* China Meteorological Press, Beijing, 233 pp. (in Chinese)

Zhao Yuchun, Wang Renqiao, Zheng Qisong, et al., 2003: Mesoscale analysis of a heavy rainfall over the middle valleys of Changjiang River. *Meteor. Monthly*, **29**(11), 14-19. (in Chinese)

Zhang Hua, Xue Jishan, Zhuang Shiyu, et al., 2004: Idea experiments of GRAPES three-dimensional variational data assimilation system. *Acta Meteor. Sinica*, **62**(1), 31-41. (in Chinese)

Zhang Peichang, Dai Tiepi, Fu Desheng, et al., 1992: Principle and accuracy of adjusting the area precipitation from digital weather radar through variational method. *Chinese J. Atmos. Sci.*, **16**(2), 248-256. (in Chinese)